Simulation of Rotor Blade Element Turbulence

R. E. McFarland and Ken Duisenberg

January 1995

Simulation of Rotor Blade Element Turbulence

R. E. McFarland, Ames Research Center, Moffett Field, California
Ken Duisenberg, SYRE, SYSCON Corporation, Falls Church, Virginia

Simulation of Rotor Blade Element Turbulence

R. E. MCFARLAND AND KEN DUISENBERG[*]

Ames Research Center

Summary

A turbulence model has been developed for blade-element helicopter simulation. This model, called Simulation of Rotor Blade Element Turbulence (SORBET), uses an innovative temporal and geometrical distribution algorithm that preserves the statistical characteristics of the turbulence spectra over the rotor disc, while providing velocity components in real time to each of five blade-element stations along each of four blades.

An initial investigation of SORBET has been performed using a piloted, motion-based simulation of the Sikorsky UH60A Black Hawk. Although only the vertical component of stochastic turbulence was used in this investigation, vertical turbulence components induce vehicle responses in all translational and rotational degrees of freedom of the helicopter.

The single-degree-of-freedom configuration of SORBET was compared to a conventional full 6-degrees-of-freedom baseline configuration, where translational velocity inputs are superimposed at the vehicle center of gravity, and rotational velocity inputs are created from filters that approximate the immersion rate into the turbulent field. For high-speed flight the vehicle responses were satisfactory for both models. Test pilots could not distinguish differences between the baseline configuration and SORBET. In low-speed flight the baseline configuration received criticism for its high frequency content, whereas the SORBET model elicited favorable pilot opinion.

For this helicopter, which has fully articulated blades, results from SORBET show that vehicle responses to turbulent blade-station disturbances are severely attenuated. This is corroborated by in-flight observation of the rotor tip path plane as compared to vehicle responses.

The Simulation

A piloted simulation was performed on NASA Ames Research Center's Vertical Motion Simulator (VMS) in 1994 using the GENHEL UH60A Black Hawk math-

---
[*]SYRE, SYSCON Corporation, 8110 Gatehouse Rd., Falls Church, VA 22042.

ematical model of reference 1 as a platform to investigate the Simulation of Rotor Blade Element Turbulence (SORBET) model. This was a simulation technology experiment designed for the purpose of evaluating the influence of stochastic turbulence created at the blade-element stations of a rotor system.

This project was conducted primarily to determine if a representative workload could be accommodated by our computer system in real time, and to ascertain whether the cyclostationary (periodically stationary) effects of reference 2 were significant in the motion environment of the VMS. Favorable pilot opinion was somewhat surprising because independent longitudinal and lateral inputs were not used during the piloted runs. Furthermore, angular components of turbulence were not explicitly included in SORBET, but rather occurred as induced responses from the superposition of vertical components at the blade stations.

The complete SORBET-Black Hawk model, including all the requisite motion and visual communication software, was executed on a single processor (VAX 9000) with a cycle time of 12 milliseconds. Cyclic phenomena are generally experienced in blade-element rotor models. The introduction of turbulence did not amplify these effects.

For the initial proof-of-concept simulation, only the vertical component of turbulence was used. Although pilots recognized the absence of the horizontal disturbances under certain flight conditions, their comments were generally quite favorable concerning the vehicle performance in turbulence. As opposed to the conventional body-fixed approach to turbulence modeling, SORBET has, at least incrementally, improved realism.

The SORBET Model

For implementation into the GENHEL UH60A mathematical model of reference 1, an heuristic model of turbulence (SORBET) was developed that preserves the Gaussian statistical characteristics of turbulence filters over the rotor disc. This model avoids the large computational and storage requirements of recent investigations into rotorcraft turbulence models (refs. 2 and 3), and imposes a modest computational overhead. SORBET was designed to create and propagate all three translational

components of MIL SPEC turbulence (ref. 4) in real time. The turbulence velocity components are superimposed at each blade-element location as a function of vehicle velocity, with distribution according to the element's instantaneous geometry.

Recent advances in the computational capacity of the simulation facility were significant in the decision to develop a model that distributes turbulence over the rotor disc. This was anticipated in reference 5:

> Progressive gust penetration by the rotor is an important feature which should be included, where possible, as it is likely to strongly influence the simulation results. Consequently, the individual blade mode with the gust field model should be used when high computation time is permissible.

The entire stochastic rotor-element turbulence model is described here, although for the initial proof-of-concept simulation only the vertical component of turbulence was used. Examples from this model are presented for the helicopter in low-speed flight (10 knots).

In this study the Dryden spectral form was selected due to its computational efficiency, although a discrete model of a curve-fit approximation to the von Karman form[1] does not offer any particular technical challenge. As will be discussed, the rotor-to-body attenuation is so severe that the original gust spectra appear to be of secondary consideration. From reference 4, "When no comparable structural analysis is performed or when it is not feasible to use the von Karman form, use of the Dryden form will be permissible." The difference between the Dryden and von Karman form is basically a small variation in the high frequency content (ref. 6).

SORBET Model Assumptions

Conventional MIL SPEC angular turbulence filters are a substitute for the finite-element distribution of translational turbulence in the air mass over the airframe. In the current study only the rotor disc is considered as an airframe, and the translational turbulence in the air mass is distributed over the rotor disc to each blade element. This distribution produces rotor moments as well as forces. Hence, only the MIL SPEC translational turbulence filters were used in the SORBET model.

From Taylor's hypothesis, the turbulent flow is stationary and homogeneous in the longitudinal direction. Turbulence filter outputs are statistically valid at either

fixed spatial locations or at points translating with the vehicle (as is the case in the conventional body-fixed formulation). Two points of applicability are selected along an onset line that is perpendicular to the vehicle flightpath, and tangential to the leading edge of the rotor disc.

The outputs of turbulence filters are applicable at points on the onset line at the discrete time points. Interpolation perpendicular to the onset line requires a transport delay that is proportional to the distance along the flightpath to the element location, and inversely proportional to the vehicle's aerodynamic velocity.

Simulating transport delays requires that the turbulence filter outputs be tabled, and updated each computer cycle. A practical limit on the table size produces a corresponding minimum velocity of propagation through the rotor disc in simulation.

The MIL SPEC translational filters contain a pole proportional to the aerodynamic velocity. This velocity is limited to the value determined from the selected table size.

The turbulence is assumed uncorrelated at each side of the rotor disc, and homogeneous in the lateral dimension. The statistical properties of the turbulence are then invariant over the entire rotor disc by using what we call Gaussian interpolation between values applicable on each side of the rotor disc.

Geometrical Considerations

The Black Hawk rotor system has four blades ($N = 4$). For each of the blades the number of segments used in the simulation was five ($M = 5$). The blade and segment indices are defined

$$1 \le n \le N \quad \text{(blades)}$$

$$1 \le m \le M \quad \text{(segments)}$$

Using the equal-annuli algorithm of reference 1, the radii to the blade stations may be computed from

$$r_m = \sqrt{(e+e')^2 + \frac{\left(m-\frac{1}{2}\right)}{M}\left[R^2 - (e+e')^2\right]} - e$$

where the rotor radius is $R = 26.83$ ft, the hinge offset is $e = 1.25$ ft, and the spar length is $e' = 2.25$ ft.

The azimuth angle of the nth blade with respect to the vehicle's aft centerline is given by

---

[1]The earliest edition of such a model that we have discovered is in an unpublished Boeing document (YC-14-FC-111R) by James H. Vincent in December 1973.

$$\psi_n = \int \Omega dt + 2\pi\left(\frac{n-1}{N}\right)$$

where $\Omega = 27$ rad/sec is the nominal rotor RPM.

In the SORBET model, rather than defining the translational disturbance velocities at the vehicle center of gravity, they are defined at two onset points, located along an onset line that is perpendicular to the horizontal mean wind vector v_H shown in figure 1. Using Gaussian inputs, three independent turbulence velocity histories are computed at each of these two points, in real time. These histories are updated each cycle time, and the pertinent values from these histories are distributed to the individual segment locations by temporal and geometrical algorithms.
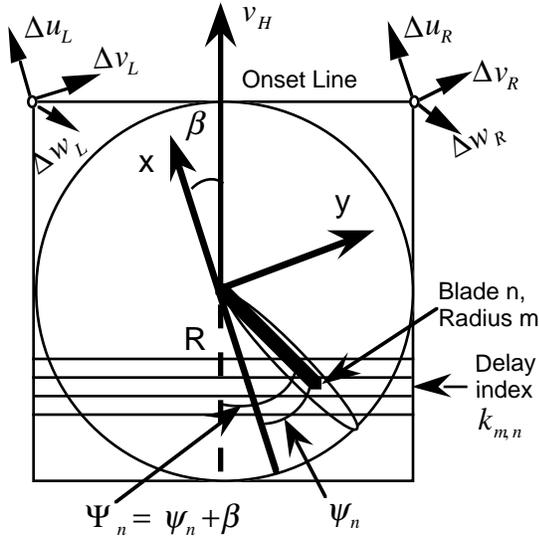
Figure 1. Rotor geometry.

Where u_b is the vehicle's longitudinal aerodynamic velocity and v_b is the lateral aerodynamic velocity, the in-plane aerodynamic velocity may be defined (approximately) by

$$v_H = \sqrt{u_b^2 + v_b^2}$$

Using this velocity and the sideslip angle β, the perpendicular onset line is as shown in figure 1. The aerodynamic azimuth angle (wind axis) for the nth blade is then

$$\Psi_n = \psi_n + \beta$$

where ψ_n is the nth blade's geometrical azimuth angle from aft.

This geometry is shown below to be sufficient to establish both the longitudinal and lateral distributions.

Longitudinal Distribution

The left and right Dryden filters receive Gaussian inputs, so the outputs of these linear filters are also Gaussian. Furthermore, a transport delay in these outputs does not alter the statistical characteristics. The outputs of the filters are stored in tables, which are updated each cycle time. The value applicable for a given element is determined by selecting a value from the tables. Given that the table size is established ($K_M = 500$) for storing time histories of the outputs of the filters, the minimum aerodynamic velocity $v_{\min}$ that may be accommodated is determined by distributing the table over the rotor diameter.

$$v_{\min} = \frac{2R}{K_M \Delta t}$$

If a smaller minimum velocity is required, a larger table size must be selected. For the SORBET simulation cycle time $\Delta t = 0.012$ sec, the minimum velocity for $K_M = 500$ is 8.944 ft/sec (5.3 knots). The rotor-plane aerodynamic velocity used in the turbulence filters is restricted to this minimum.

$$v_{uv} = \begin{cases} v_{\min} & v_H < v_{\min} \\ v_H & v_H \geq v_{\min} \end{cases}$$

Independent of vehicle velocity, exactly $K_M \Delta t = 6$ sec of data are stored in the tables. Time histories of the outputs of six turbulence filters are contained in six separate tables, each of length K_M. At the minimum velocity the individual cells correspond to a length of 0.10732 ft (such that 500 of them span the rotor diameter), whereas at a velocity of 100 ft/sec (59.2 knots), for example, the cells are each 1.2 ft long such that only 45 of them are needed to span the rotor diameter.

In order to select the velocities to be used from the tables, for any blade element an integer index is computed to determine the element's perpendicular distance from the onset line. Defining

$$r_{m,n} = R + r_m \cos \Psi_n$$

the index is given by

$$k_{m,n} = \left\lceil \frac{r_{m,n}}{v_{uv} \Delta t} \right\rceil$$

where the upper brackets denote the integer ceiling operation. The tables extend beyond the rotor disc for higher vehicle velocities than the minimum, such that stationary outputs are available for table size increases caused by decreases in velocity. The hypothetical case

3

where the entire rotor disc receives the same table value could only occur for velocities in the thousands of knots.

Lateral Distribution

Having determined the longitudinal point of application (or index $k_{m,n}$) for a given rotor element, the turbulence velocities from the tables are identified as applicable at both the left and right sides of the rotor disc. Lateral interpolation must be used to determine the element's final turbulence velocities. Although the lateral proportion (from the left-hand side) to an element may then be determined from the geometry of figure 1

$$p_{m,n} = \frac{1}{2} + \frac{r_{m,n} \sin \Psi_n}{2R}$$

this proportion cannot be applied in a linear fashion. Using the vertical dimension, for example, although both $\Delta w_L(k_{m,n})$ and $\Delta w_R(k_{m,n})$ are Gaussian random variables with zero mean and RMS value given by σ_w, in order to preserve the statistical properties over the rotor disc we use Gaussian interpolation, so that the combination retains the same variance (and all other moments) as the original Gaussian variables.

A variable x is normally distributed with zero mean and variance σ^2 when its density function is

$$f(x) = \frac{1}{\sigma\sqrt{2\pi}} e^{-\frac{1}{2}(x/\sigma)^2}$$

The variance is defined by

$$E[x]^2 = \int_{-\infty}^{\infty} x^2 f(x) dx = \sigma^2$$

for a single random variable. When we combine two independent random variables at some interior point, we must consider their proportion p.

When a proportion p has the range $(0 \le p \le 1)$, as it does in $p_{m,n}$ above, a linear combination of two normally distributed variables may be forced to have the same statistical properties as the originals by normalizing the density functions as follows:

$$f(x_1) = \frac{p}{\sqrt{p^2 + (1-p)^2}} f(x)$$

$$f(x_2) = \frac{1-p}{\sqrt{p^2 + (1-p)^2}} f(x)$$

As applied to variables with a zero mean value, this is a consequence of the arithmetic mean theorem given in reference 7, where

$$E\left[\frac{px_1}{\sqrt{p^2 + (1-p)^2}} + \frac{(1-p)x_2}{\sqrt{p^2 + (1-p)^2}}\right]^2 =$$

$$E\left[\frac{p^2 x_1^2 + (1-p)^2 x_2^2 + 2p(1-p)x_1 x_2}{p^2 + (1-p)^2}\right] =$$

$$E\left[\frac{p^2 x_1^2 + (1-p)^2 x_2^2}{p^2 + (1-p)^2}\right] = \sigma^2$$

because $E[x_1 x_2] = 0$ for independent variables, and $E\left[x_1^2\right] = E\left[x_2^2\right] = \sigma^2$. The variance of the combined distribution then remains σ^2. Gaussian interpolation is therefore given by

$$\Delta w_{m,n} = \frac{p_{m,n}\Delta w_R(k_{m,n}) + (1-p_{m,n})\Delta w_L(k_{m,n})}{\sqrt{p_{m,n}^2 + (1-p_{m,n})^2}}$$

This combination is applicable for all three translational velocity components at an element location.

The Dryden Model

From reference 4 the low-altitude vertical turbulence scale length is given as a piecewise continuous function of altitude h

$$L_w = \begin{cases} 10 & h < 10 \text{ ft} \\ h & 10 \le h \le 1000 \text{ ft} \\ 1000 & h > 1000 \text{ ft} \end{cases}$$

and the in-plane components are given by the functions

$$L_u = L_v = \begin{cases} 75.64 & h < 10 \text{ ft} \\ hf_{uv}^{-1.2} & 10 \le h \le 1000 \text{ ft} \\ 1000 & h > 1000 \text{ ft} \end{cases}$$

where

$$f_{uv} = 0.177 + 0.000823h$$

The horizontal turbulence RMS intensities are a function of the selected vertical turbulence intensity σ_w

$$\sigma_u = \sigma_v = \sigma_w f_{uv}^{-0.4}$$

The results shown in this paper are for $\sigma_w = 5$ ft/sec, $h = 200$ ft, and $v_H = 16.9$ ft/sec (10 knots).

Using Taylor's frozen field hypothesis from reference 4, the Dryden form of the linear turbulence transfer functions are given by

$$\Delta u(s) = \frac{\sigma_u \sqrt{2v_{uv}/\pi L_u}}{s + v_{uv}/L_u}$$

$$\Delta v(s) = \frac{\sigma_v \sqrt{v_{uv}/\pi L_v}\left(\sqrt{3}s + v_{uv}/L_v\right)}{\left(s + v_{uv}/L_v\right)^2}$$

$$\Delta w(s) = \frac{\sigma_w \sqrt{v_{uv}/\pi L_w}\left(\sqrt{3}s + v_{uv}/L_w\right)}{\left(s + v_{uv}/L_w\right)^2}$$

For conventional aircraft (and our baseline configuration of the UH60A) the angular transfer functions are developed from partial differential equations relating these translational disturbances to the immersion rate of the vehicle into the turbulent field. These equations use a parameter b, which is the wingspan length of the aircraft.

$$\Delta p(s) = \frac{\sigma_w \left(\dfrac{\pi}{4b}\right)^{7/6} \sqrt{0.8v_{uv}}}{L_w^{1/3}\left(s + \dfrac{\pi v_{uv}}{4b}\right)}$$

$$\Delta q(s) = \frac{\dfrac{\pi}{4b}s\,\Delta w(s)}{s + \dfrac{\pi v_{uv}}{4b}}$$

$$\Delta r(s) = \frac{\dfrac{\pi}{3b}s\,\Delta v(s)}{s + \dfrac{\pi v_{uv}}{3b}}$$

These angular disturbances are not used in the SORBET model because the geometry is considered in the points of application of the translational turbulence excitations. The asymmetric turbulence velocities produce moments, which in turn produce angular activity.

All of the baseline case transfer functions have been presented because their spectra are displayed on certain graphs herein for reference purposes. Also, this baseline model is actually available as an option in our UH60A simulation model, and was used by pilots for comparison purposes.

Discrete Implementation

Continuous transfer functions involving random inputs are typically converted to discrete form using the zero-order hold formulation, where the input is assumed constant over each computer cycle Δt. The z-transforms of Laplace functions $f_i(s)$ then become

$$F_i(z) = Z\left\{\left(\frac{1-e^{-s\Delta t}}{s}\right)f_i(s)\right\}$$

which may then be converted to difference equations for discrete implementation. This process is nicely explained in reference 8.

Using this technique on the Dryden transfer functions produces the coefficients

$$\gamma_u = v_{uv}\Delta t/L_u$$

$$f_1 = e^{-\gamma_u}$$

$$f_2 = \sigma_u(1 - f_1)\sqrt{2/\gamma_u}$$

$$\gamma_v = v_{uv}\Delta t/L_v$$

$$g_1 = 2e^{-\gamma_v}$$

$$g_2 = -e^{-2\gamma_v}$$

$$g_3 = \left[\sigma_v/\sqrt{\gamma_v}\right]\left[1 - e^{-\gamma_v} + \left(\sqrt{3}-1\right)e^{-\gamma_v}\gamma_v\right]$$

$$g_4 = -\left[\sigma_v e^{-\gamma_v}/\sqrt{\gamma_v}\right]\left[1 - e^{-\gamma_v} + \left(\sqrt{3}-1\right)\gamma_v\right]$$

$$\gamma_w = v_{uv}\Delta t/L_w$$

$$h_1 = 2e^{-\gamma_w}$$

$$h_2 = -e^{-2\gamma_w}$$

$$h_3 = \left[\sigma_w/\sqrt{\gamma_w}\right]\left[1 - e^{-\gamma_w} + \left(\sqrt{3}-1\right)e^{-\gamma_w}\gamma_w\right]$$

$$h_4 = -\left[\sigma_w e^{-\gamma_w}/\sqrt{\gamma_w}\right]\left[1 - e^{-\gamma_w} + \left(\sqrt{3}-1\right)\gamma_w\right]$$

These coefficients are used in the following six difference equations, each driven by an independent Gaussian noise source η_i, with a zero mean value and a unity standard deviation.

$$\Delta u_L(k) = f_1\Delta u_L(k-1) + f_2\eta_1(k)$$

$$\Delta u_R(k) = f_1\Delta u_R(k-1) + f_2\eta_2(k)$$

$$\Delta v_L(k) = g_1\Delta v_L(k-1) + g_2\Delta v_L(k-2)$$
$$+ g_3\eta_3(k) + g_4\eta_3(k-1)$$

$$\Delta v_R(k) = g_1\Delta v_R(k-1) + g_2\Delta v_R(k-2)$$
$$+ g_3\eta_4(k) + g_4\eta_4(k-1)$$

$$\Delta w_L(k) = h_1 \Delta w_L(k-1) + h_2 \Delta w_L(k-2)$$

$$+ h_3 \eta_5(k) + h_4 \eta_5(k-1)$$

$$\Delta w_R(k) = h_1 \Delta w_R(k-1) + h_2 \Delta w_R(k-2)$$

$$+ h_3 \eta_6(k) + h_4 \eta_6(k-1)$$

These computationally efficient equations produce stable outputs for all stable inputs.

For the body-fixed formulation these velocities are super-imposed at the center of gravity. In SORBET these velocities are created at the two onset points and then dis-tributed and superimposed at the various blade-element locations. They produce forces and moments because they modify the angle of attack of each element.

Element Velocities

Forces developed at individual blade-element locations are invariably summed to create total rotor forces and moments. In this section the spectral filtering conse-quences of the summation operation are illustrated by using the turbulence velocities themselves. Then, in the next few sections, this is further illustrated using the blade flapping spectra and the total vehicle responses. Although a blade variable may exhibit much harmonic content, the summation over the blade index effectively removes many of the harmonics (ref. 9).

Figure 2 displays typical time histories of vertical turbulence produced at the two onset points ($\Delta w_L, \Delta w_R$). These histories are the uncorrelated outputs of the Dryden vertical filters, excited by Gaussian noise with $\sigma_w = 5$ ft/sec.

The velocities of figure 2 are the origins of the turbulence velocities for each blade element. In response to these inputs, figure 3 is an example of the velocity of just one element (outboard, $m = 5$) of one blade.
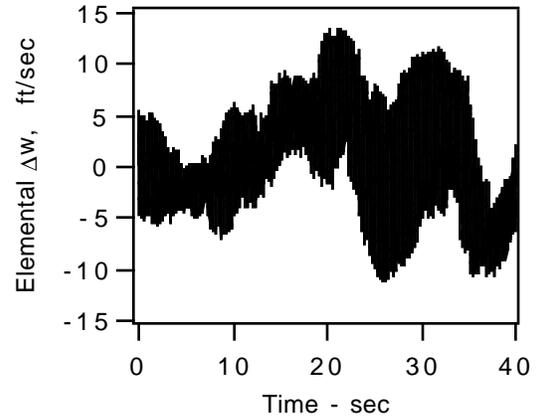
Figure 3. Element velocity.

Because the velocities at an element are rotationally sampled, figure 3 displays considerable one-per-rev fre-quency content, bounded approximately by the input curves shown in figure 2.

Each and every element experiences vertical velocities similar to that shown in figure 3. However, the summa-tion of all of the 20 elements for each time point selec-tively eliminates most of the high frequency content. Figure 4 displays this phenomenon. What remains after summation is essentially the average of the original onset velocities.

Figure 2. Onset point velocities.
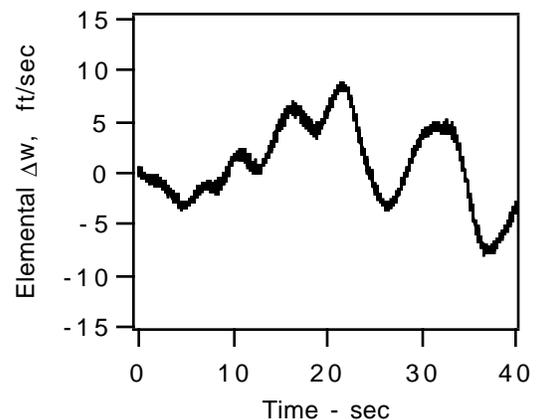
Figure 4. Summed velocities.

This phenomenon occurs independent of turbulence. In the next three sections this is further illustrated using both rotor and vehicle variables.

Rotating Frame Blade Spectra

The flight condition documented here is for a trimmed vehicle in 10-knot horizontal flight at an altitude of 200 ft. Under these conditions, when turbulence is not present, any given blade produces the flapping (β_n of ref. 1) time history as shown in figure 5.
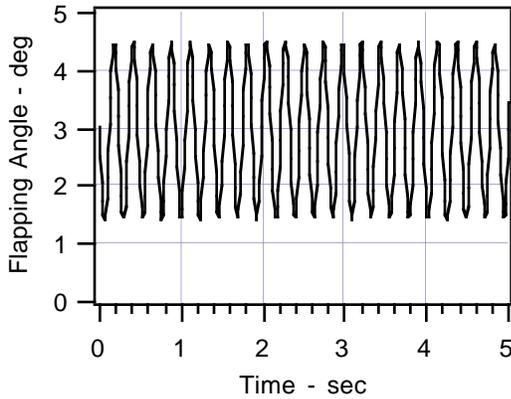
Figure 5. Flapping without turbulence.

The power spectral density (PSD) or autospectrum of this signal is shown in figure 6.
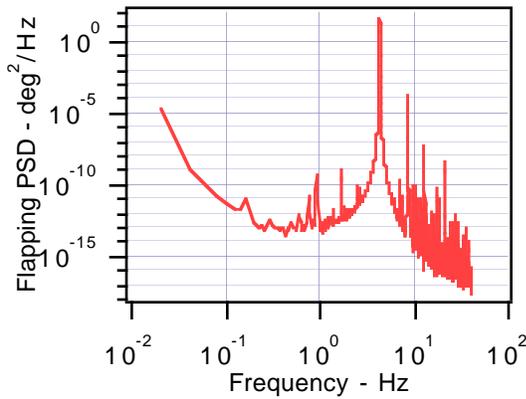
Figure 6. Flapping PSD without turbulence.

The significant frequencies at the blade level of examination are the blade harmonics, beginning with the fundamental, at 4.297 Hz (27 rad/sec). These harmonics theoretically extend to infinity. Frequencies on this graph that are observed below the fundamental are, for the most part, aliased harmonics (originating beyond the Nyquist frequency).

When the vertical turbulence ($\sigma_w = 5$ ft/sec) is introduced into the rotor system under the same conditions, the time history of a blade displays more frequency content, as indicated in figure 7.
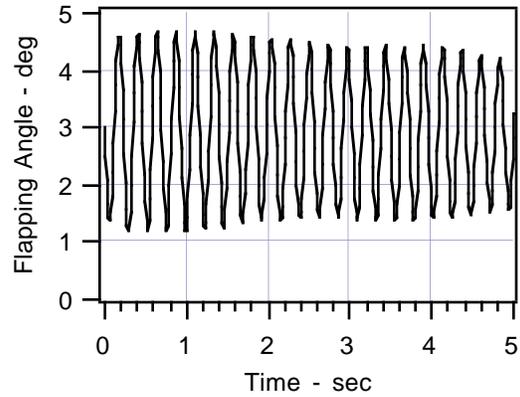
Figure 7. Flapping with turbulence.

The background spectrum of figure 6 is then elevated by a few orders of magnitude, as shown in figure 8.
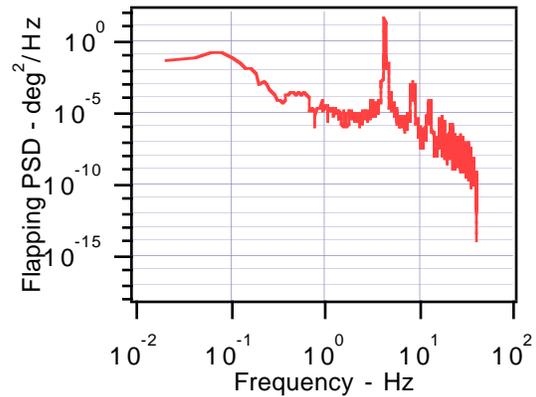
Figure 8. Flapping PSD with turbulence.

The significant periodic components in these spectra are created by the blades essentially tracking each other, independent of turbulence. Turbulence elevates the background spectrum, but since the inputs are not uniform over the rotor disc it does not have a significant influence on the rotor harmonics. Notice that in figure 8, except for the first harmonic, the blade harmonics almost disappear into the turbulent background, and they are not amplified by the introduction of turbulence. This leads to the conclusion that at the blade level of consideration the introduction of turbulence does not produce significant cyclostationary phenomena.

The lagging spectrum is not shown here. At this flight condition it is about an order of magnitude smaller than the flapping spectrum.

Fourier Coefficients

Forces and moments generated by blade activity are transmitted to the airframe through summation functions. Given that each simulated blade has identical physical properties, such as mass, length, and relationship to adjacent blades, the consequence of summation is to eliminate all integer harmonic multiples of the RPM that are not a multiple of the number of blades (ref. 9). This is illustrated by considering the principal flapping Fourier coefficients.

The principal flapping Fourier coefficients (main distortions of the rotor plane, in nonrotating frame) are given by the following summations of the individual flapping angles (β_n of ref. 1).

$$A_{0F} = \frac{1}{N} \sum_{n=1}^{N} \beta_n$$

$$A_{1F} = -\frac{2}{N} \sum_{n=1}^{N} \beta_n \cos \psi_n$$

$$B_{1F} = -\frac{2}{N} \sum_{n=1}^{N} \beta_n \sin \psi_n$$

where A_{0F} is the coning (steady flapping) angle, A_{1F} is the longitudinal first harmonic, and B_{1F} is the lateral first harmonic.

The PSDs of these Fourier coefficients are given in figures 9–11. The lower lines show the behavior without turbulence, and the upper lines show the behavior with vertical rotor turbulence. In comparing these figures with figures 6 and 8 it is seen that only blade harmonics that are a multiple of the number of blades survive the summation operation, whereas the stochastic contributions are retained in the spectra of the rotor disc.
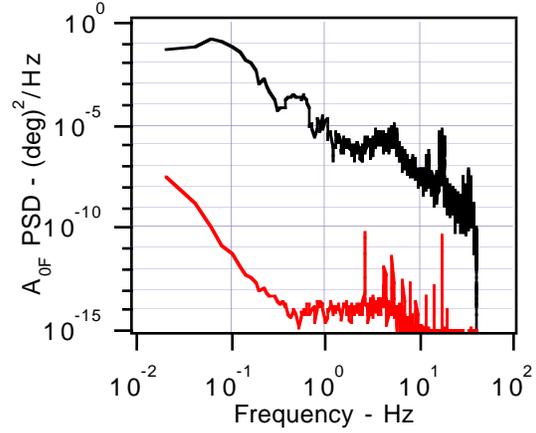
Figure 9. A_{0F} spectra.
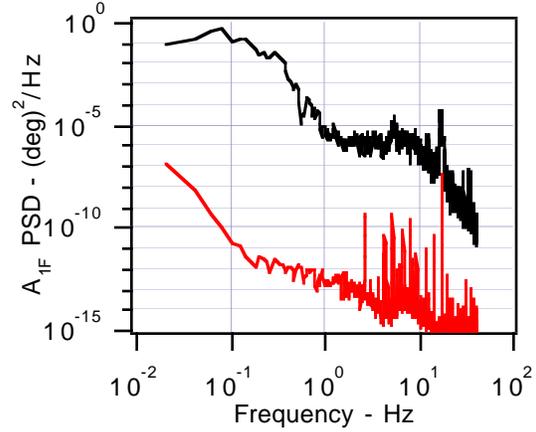
Figure 10. A_{1F} spectra.
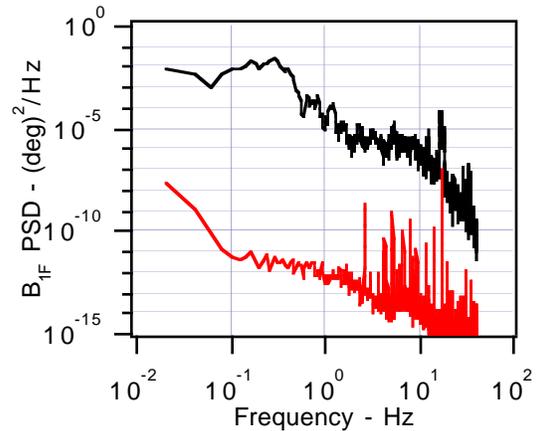
Figure 11. B_{1F} spectra.

8

Harmonics of N/rev seen in these figures are not caused by turbulence (see ref. 9). They are a normal consequence of blade summation of periodic phenomena. Of course, interior harmonics will be observed if the blades are not tracking each other in their rotational environment. This occurs during transients, and is also a consequence of mismatched blades:

> The one-per-revolution (27 rad/sec) frequency content that can be seen in the flight-test data is caused by a mismatched rotor blade that was not tracking with the other three on the test aircraft; therefore, this frequency is not observed in the simulation results. (ref. 10)

Baseline Traces

The baseline spectra are the responses for the conventional implementation of turbulence, typically used for fixed-wing aircraft but also available in our UH60A model. In the baseline configuration the inputs are at the vehicle center of gravity. The transfer functions for this formulation were presented in the section named The Dryden Model. The baseline spectra also describe the outputs of SORBET's right and left filters.

The baseline configuration has been available for the UH60A model (and other helicopters) for a number of years, although pilots have invariably been critical of its performance during low-speed flight. This baseline configuration is nonetheless interesting for comparison purposes. In figure 12 the vertical velocity baseline spectra are shown, with parameter a = v/L_w.
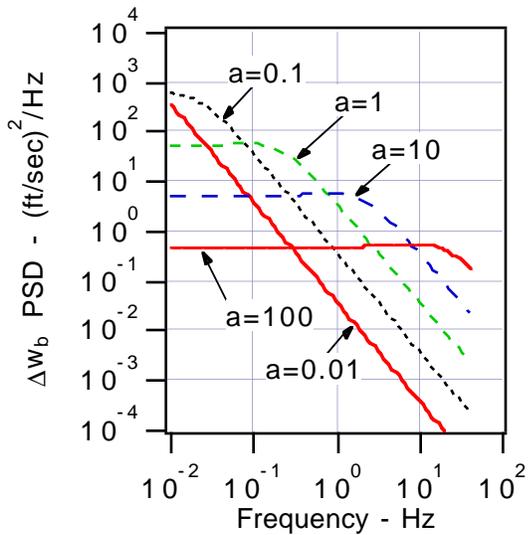
Figure 12. Baseline spectra.

For the flight condition of 10 knots at an altitude of 200 ft, the parameter is about 0.04.

At the 10-knot flight condition the baseline PSDs are presented in figures 13–18 as dotted lines. In the configuration studied here only the vertical axis of SORBET had an input. However, all axes (solid lines) display outputs.
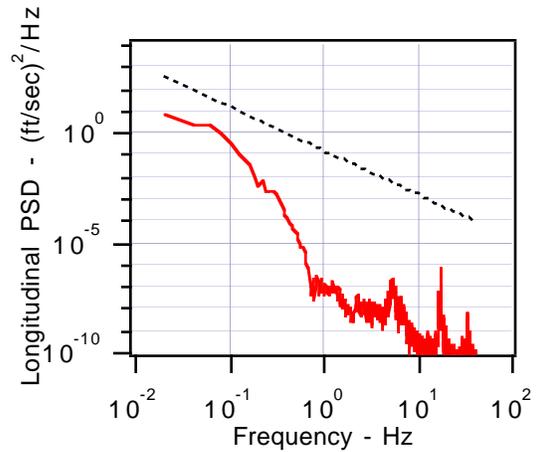
Figure 13. Δu_b, vertical input.

Figure 14. Δv_b, vertical input.

9
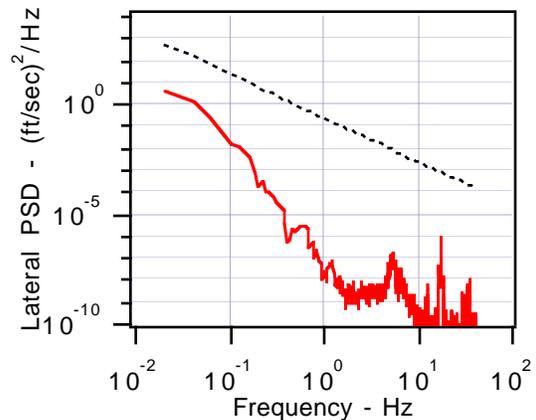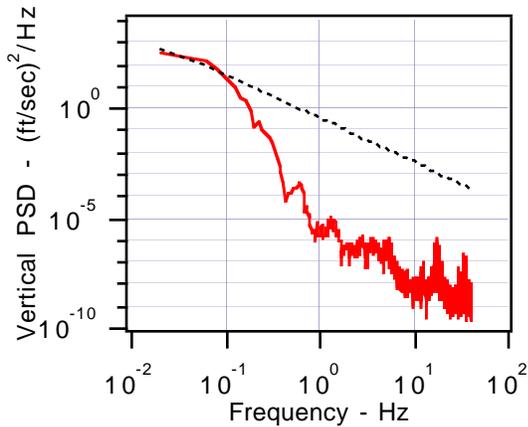
Figure 15. Δw_b, vertical input.
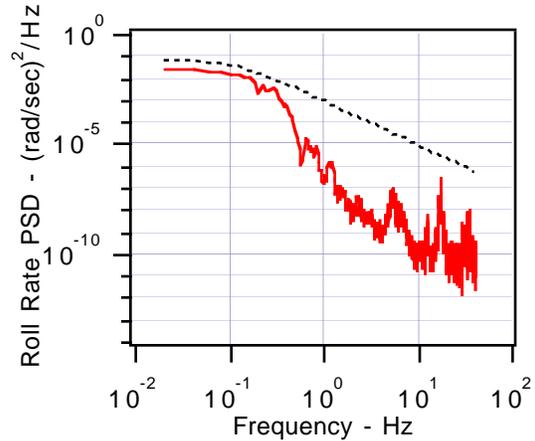
Figure 16. Δp_b, vertical input.

It is useful to think of the body-fixed spectra (dotted lines) as representative of the *velocity of the air mass, as experienced by a point traversing through it.* If this air mass velocity is rigidly attached to the vehicle, as it is in the conventional formulation, then the vehicle itself experiences this velocity. If, however, it is attached to the velocity of a blade element, then it produces an alteration in that element's angle of attack, which in turn contributes to the production of rotor-system forces and moments.

The body-fixed baseline spectra could only be the same as the helicopter spectra if unity transfer functions existed from the rotor to the body. Indeed, the existence of nonunity transfer functions in this regard is obvious because rotorcraft responses differ from those of conventional aircraft. Nonetheless, these spectra are useful in determining just what the rotor-to-body effects are. Only "for high speed flight, where helicopters behave more like conventional aircraft"[2] could these dotted baseline curves possibly represent desirable responses.

For completeness the angular PSDs are also shown in figures 16–18. All angular disturbances observed in SORBET were induced responses from the application of vertical turbulence. The baseline curves on these plots were obtained from the conventional transfer functions, using an arbitrary value of wingspan length b of 20 ft.
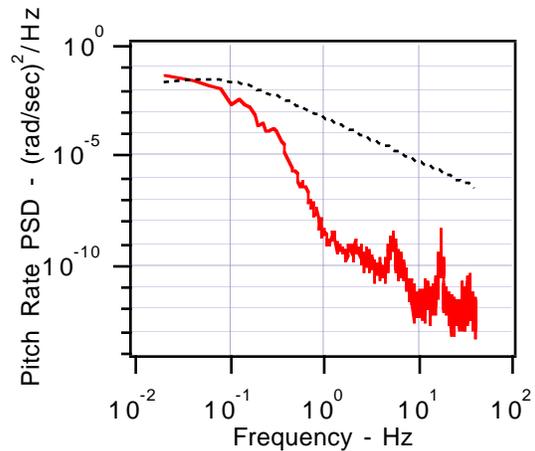
Figure 17. Δq_b, vertical input.
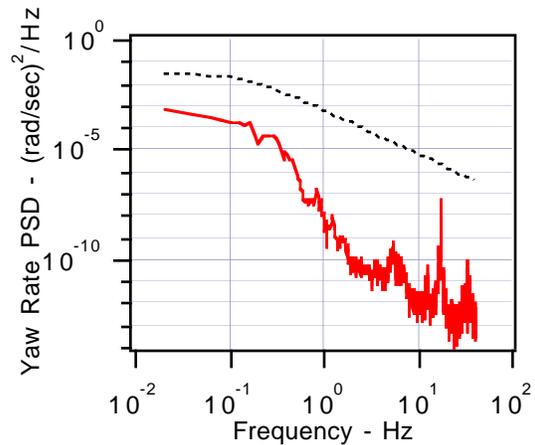
Figure 18. Δr_b, vertical input.

---

[2]Remark by Norman D. Ham of Massachusetts Institute of Technology during his class on Aerodynamics, Stability, and Control of Rotorcraft and Other VTOL Aircraft, Ames Research Center, 1978.

In figures 13–18 only the vertical component of turbulence into the rotor system was used, as was the case during pilot evaluations. Induced effects are seen to occur on all other axes. Pilots generally concurred that this system felt quite realistic, with the exception that some airspeed and lateral variations were lacking. This is illustrated in figures 13 and 14.

Rotor-Airframe Transfer Function

In figure 15 the vertical vehicle response to vertical rotor turbulence was shown. Since the dotted line represents the spectral input throughout the rotor disc, clearly much energy is lost in the rotor-to-body transfer function. This transfer function was determined by emulating a single-input/single-output (SISO) system using the same statistical value for each element at each time point.

The baseline vertical Dryden PSD as shown in figure 15 is plotted in figure 19 as a dashed line. Using identical random inputs at each element, the SISO PSD curve of figure 19 was created. Comparing the SISO curve to the input spectrum of the air mass (dashed line), there is considerable attenuation. Also shown in figure 19 is the multiple-input/single-output (MISO) PSD curve, as replicated from figure 15. More attenuation occurs on this curve, when the inputs are not uniform (MISO) throughout the rotor disc.
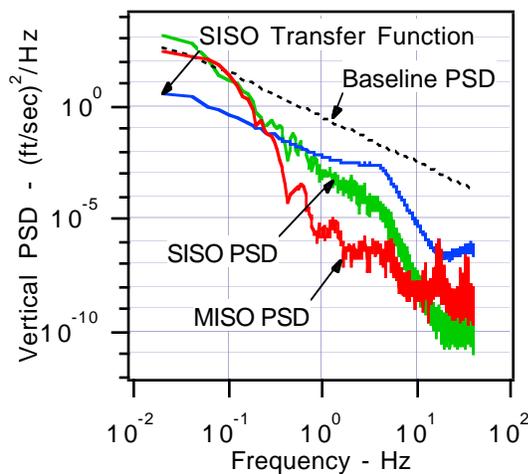
Figure 19. Δw_b, same vertical inputs.

The rotor-to-body transfer function (nondimensional) is also shown in figure 19, as computed from the SISO curve with respect to the baseline curve. The attenuation becomes more pronounced beyond about 4.3 Hz, which happens to be the rotor RPM. This phenomenon is a consequence of the blade summation process operating on signals that are identical for each element.

When turbulence was permitted to vary over the rotor disc according to the algorithms, the slightly different results of figure 15 were produced, shown in figure 19 as the MISO curve. The transfer function for the MISO system has not been identified, although it must be similar to the SISO system given in figure 19 because of the vehicle response similarities shown by the SISO and MISO curves.

Pilot Opinion

From figure 19, the rotor system clearly attenuates high-frequency nonuniform inflow (as in blade-element turbulence) to a greater extent than it attenuates uniform inflow. Nonetheless, lower frequency distortion of the rotor disc caused by turbulence may be an important piloting cue. Distortions are an indication of activity in the stability augmentation system (SAS), and may influence speed selection. Some of the simulation pilots stated that in real helicopter flight they sometimes "observed the rotor plane undergoing large responses to turbulence, while the airframe's motion was relatively smooth." In response to pilot requests for this visual cue, the tip-path plane will be included in the visual display for the next rotorcraft simulation on the VMS.

To assure that simulation pilots had similar conditions in which to assess the model, they were given identical tasks of following recorded flightpaths. Our chief test pilot for the simulation established these basic paths (without turbulence) by flying a set of runs over the terrain, and the spatial positions and orientations of the helicopter were recorded. Using a sophisticated playback feature of our heads-up display, other pilots were shown these paths by using both a graphical lead aircraft and a visually superimposed stick-figure canyon (ref. 11). This is depicted in figure 20, where both the lead aircraft and the velocity vector (circle) are indicated.
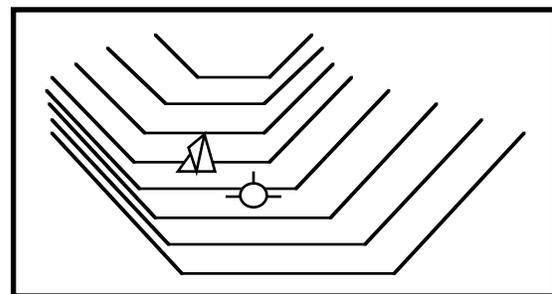
Figure 20. Playback canyon.

Pilots had the task of following the lead aircraft (at speed) and staying within the canyon. Without turbulence, this task was quite simple for all pilots. The task became more difficult when turbulence was added.

All pilots found the SORBET model realistic, and their comments were used to improve the model during the simulation.

Pilots generally agreed that the turbulence magnitude should be a function of velocity. Above 40 knots, the subjective values for light and moderate turbulence were selected as $\sigma_w = 5$ ft/sec and 8 ft/sec, respectively. Near hover, pilots selected standard deviations that were half these values. The reason for this is unknown, and should be investigated further. Although the frequency content is acceptable, the magnitude must be decreased in low-speed flight. For the body-fixed formulation in low-speed flight, pilots invariably criticized the baseline configuration. A typical comment was "It was like a washboard."

Pilots are clearly sensitive to the more nonlinear aspects of atmospheric turbulence. From reference 12, "turbulent flows are diffusive and intermittent" and, moreover, "the element of surprise that is characteristic of turbulence must be present." Pilots were quick to point out that although the stochastic turbulence was realistic, it was too continuous and lacked occasional sharp gusts. Their comments reflected reference 13 quite closely:

> One of the most common grievances helicopter pilots have with simulated atmospheric turbulence is that it is too regular, and does not contain 'patches' of turbulence followed by periods of calm air.

Due to the large number of pilot remarks in this area, we accommodated them on certain points. During the simulation, a few additions to the SORBET model were made, as described below. The pilots agreed that these additions provided even more realism.

Occasional vertical gusts were simulated by changing the magnitude of the mean vertical wind at random times. Gusts were programmed to arrive more frequently and more abruptly at high speeds (about every 3 sec) than at low speeds (every 12 sec). The resulting random vertical gusts were praised by the pilots as extremely characteristic of real turbulence.

Moments of calm air were introduced by scaling the magnitude of the stochastic turbulence to zero for random time periods (between 2 and 6 sec). This was followed by smoothly applying random percentages of the full magnitude, also for random time periods. This technique created the effect of patches of different levels of turbulence.

With the addition of vertical gusts and patches of turbulence, the vertical turbulence was accepted by all the pilots as very realistic. One deficiency they found was in the reduced level of lateral, longitudinal, and yaw turbulence cues. Since the model did not directly influence these axes, these comments were expected. As a partial solution, a stochastic input, perpendicular to the tail rotor, was added. While the pilots noticed the extra yaw variations, they generally agreed it was not a great improvement, and the lack of lateral inputs detracted from realism.

One major pilot concern involved the way the turbulence was not correlated to the terrain. This was not within the scope of SORBET, but work is being done in this area (ref. 14).

In summary, pilot comments were quite favorable for SORBET during the 2-week motion-based simulation study. Representative comments are listed below, where the italics are the authors'.

1. The chief NASA test pilot for this simulation, Munro Dearing, commented during low-speed flight that "this would be typical of light-to-moderate gusts in hover." However, at 100 knots he noticed "there is a lack of heave." These comments were made prior to the introduction of the embellishments described above.

2. NASA test pilot Bill Hindson commented on SORBET once the occasional gusts were included that "the low frequency pitch and roll *felt* is also characteristic *of turbulence*," and "it is a fairly realistic simulation."

3. NASA test pilot Tom Reynolds commented on SORBET when the occasional quiet periods were introduced that "*this is* much like what I expect is real," and "overall, this feels pretty good, fairly realistic light-to-moderate *turbulence*."

4. NASA test pilot Gordon Hardy commented on the SORBET simulation that "*these are* pretty typical excursions compared to real flight," but also said "I'd expect more lateral motion."

5. Retired NASA test pilot Ron Gerdes commented "*there is* nothing that I would change *in the model*."

6. Navy pilot Tim Sestak commented "this is what turbulence feels like."

In-Plane Turbulence

Although piloted runs were not made with the in-plane longitudinal and lateral turbulence options enabled, it has

been established that their inclusion would have added very little to the simulation. From reference 15, "Current articulated and semi-rigid rotors are insensitive to in-plane gusts." Our own data support this statement.

In fact, adding these in-plane components to SORBET produced changes that were too trivial to show here. For this reason we postulate that in-plane translational turbulence components should probably act at the vehicle center of gravity, just as in the conventional formulation. Of course, using these in-plane components also means that consideration should be given to correlated tail rotor responses. The tail rotor becomes much more significant when gusts are considered, rather than just stationary turbulence alone.

In our next investigation we plan to include in-plane components for turbulence that will probably be applied at the vehicle center of gravity. This proposed system has also been investigated; it produces almost identical spectral responses as those shown in figures 13–18, except that the in-plane vehicle responses of figures 13 and 14 then become superimposed with the dashed lines (as in the conventional aircraft case). This model should then include the in-plane disturbances that pilots expect.

Conclusions

Adding turbulence to the Black Hawk simulation added less than 10 percent to the required cycle time. Hence, blade-element implementations of turbulence are now feasible using modern computers.

In-plane turbulence applied at the rotor elements produces minimal vehicle responses. This is therefore an unsatisfactory technique for modeling stochastic turbulence in the horizontal plane, and would probably produce erroneous results using gust models. Hence, in-plane disturbances should probably be handled more or less as in the conventional formulation, with the inclusion of the correlated influence on the tail rotor.

The vertical component of turbulence as input at the blade radial stations produces significant differences in vehicle performance from that of conventional body-fixed techniques. The differences include considerable attenuation of higher frequencies in the vertical and all rotational axes. These phenomena elicit favorable pilot opinion, and probably identify the major difference between helicopter and conventional aircraft responses.

In establishing a uniform level of turbulence over a flight regime our test pilots preferred a standard deviation that varied linearly with velocity, roughly doubling from hover to 40 knots, where it became constant. This is an unknown phenomenon that deserves further investigation.

Also, criteria for implementing patches of different levels of turbulence should be established, because they correspond to pilot experience.

References

1. Howlett, J. J.: UH-60A Black Hawk Engineering Simulation Program: Vol. I—Mathematical Model. NASA CR-166309, Dec. 1981.

2. Prasad, J. V. R.; Riaz, J.; Gaonkar, G. H.; and Yingyi, D.: Real Time Implementation Aspects of a Rotorcraft Turbulence Simulation Method. 49th Annual Forum of the American Helicopter Society, St. Louis, Mo., May 1993, p. 459.

3. Robinson, John E.; Weber, Timothy L.; and Miller, David G.: Real-Time Simulation of Full-Field Atmospheric Turbulence for a Piloted Rotorcraft Simulator. 50th Annual Forum of the American Helicopter Society, Washington, D.C., May 1994.

4. United States Department of Defense: Flying Qualities of Piloted Aircraft. Military Specification MIL-F-8785C, Nov. 1980.

5. Dahl, H. J.; and Faulkner, A. J.: Helicopter Simulation in Atmospheric Turbulence. Vertica, vol. 3, 1979, pp. 65–78.

6. Gerlach, O. H.; van de Moesdijk, G.; and van der Vaart, J. C.: Progress in the Mathematical Modeling of Flight in Turbulence. AGARD Conference Proceedings No. 140 on Flight in Turbulence, Paper No. 5, 1973, pp. 1–38.

7. Sokolnikoff, I. S.; and Redheffer, R. M.: Mathematics of Physics and Modern Engineering. McGraw-Hill Book Co., Inc., New York, 1958, pp. 667–668.

8. Smith, J. M.: Recent Developments in Numerical Integration. Journal of Dynamic Systems, Measurement, and Control, Transactions of the ASME, No. 73-WA/Aut-6, Detroit, Michigan, March 1974.

9. McFarland, R. E.: The N/Rev Phenomenon in Simulating a Blade-Element Rotor System. NASA TM-84344, March 1983.

10. Ballin, Mark G. and Dalang-Secrétan, Marie-Alix: Validation of the Dynamic Response of a Blade-Element UH-60 Simulation Model in Hovering Flight. J. Am. Helicopter Soc., Washington D.C., May 1990, p. 84.

11. Zelenka, Richard E.; Clark, Raymond F.; and Branigan, Robert G.: Flight Test of a Low-Altitude Helicopter Guidance System with Obstacle Avoidance Capability. AGARD Avionics Panel Symposium on Low-Level and Nap-of-the-Earth Night Operations, Rome, Italy, Oct. 24–27, 1994.

12. Panofsky, Hans A.; and Dutton, John A.: Atmospheric Turbulence. John Wiley & Sons, New York, 1984, pp. 5, 278.

13. Costello, M. F.: A Theory for the Analysis of Rotorcraft Operating in Atmospheric Turbulence. Proceedings of the 46th Annual National Forum of the American Helicopter Society, Washington, D.C., May 1990, pp. 1003–1015.

14. Clement, Warren F.; and Gorder, Peter J.: Terrain-Correlated Atmospheric Turbulence Modeling for Real-Time Simulation of Nap-of-the-Earth (NOE) Flight Operations, USAAVSCOM TR 92-A-011, May 1992.

15. Judd, M.; and Newman, S. J.: An Analysis of Helicopter Rotor Response Due to Gust and Turbulence. Vertica, vol. 1, 1977, pp. 179–188.

REPORT DOCUMENTATION PAGE			Form Approved OMB No. 0704-0188

Public reporting burden for this collection of information is estimated to average 1 hour per response, including the time for reviewing instructions, searching existing data sources, gathering and maintaining the data needed, and completing and reviewing the collection of information. Send comments regarding this burden estimate or any other aspect of this collection of information, including suggestions for reducing this burden, to Washington Headquarters Services, Directorate for information Operations and Reports, 1215 Jefferson Davis Highway, Suite 1204, Arlington, VA 22202-4302, and to the Office of Management and Budget, Paperwork Reduction Project (0704-0188), Washington, DC 20503.

1. AGENCY USE ONLY *(Leave blank)*	2. REPORT DATE January 1995	3. REPORT TYPE AND DATES COVERED Technical Memorandum	
4. TITLE AND SUBTITLE Simulation of Rotor Blade Element Turbulence			5. FUNDING NUMBERS 505-64-29
6. AUTHOR(S) R. E. McFarland and Ken Duisenberg*			
7. PERFORMING ORGANIZATION NAME(S) AND ADDRESS(ES) Ames Research Center Moffett Field, CA 94035-1000			8. PERFORMING ORGANIZATION REPORT NUMBER A-950028
9. SPONSORING/MONITORING AGENCY NAME(S) AND ADDRESS(ES) National Aeronautics and Space Administration Washington, DC 20546-0001			10. SPONSORING/MONITORING AGENCY REPORT NUMBER NASA TM-108862

11. SUPPLEMENTARY NOTES
Point of Contact: R. E. McFarland, Ames Research Center, MS 243-5, Moffett Field, CA 94035-1000
(415) 604-3863
*SYRE, SYSCON Corporation, 8110 Gatehouse Rd., Falls Church, VA 22042

12a. DISTRIBUTION/AVAILABILITY STATEMENT Unclassified — Unlimited Subject Category 05	12b. DISTRIBUTION CODE

13. ABSTRACT *(Maximum 200 words)*

A piloted, motion-based simulation of Sikorsky's Black Hawk helicopter was used as a platform for the investigation of rotorcraft responses to vertical turbulence. By using an innovative temporal and geometrical distribution algorithm that preserved the statistical characteristics of the turbulence over the rotor disc, stochastic velocity components were applied at each of twenty blade-element stations. This model was implemented on NASA Ames' Vertical Motion Simulator (VMS), and ten test pilots were used to establish that the model created realistic cues.

The objectives of this research included the establishment of a simulation-technology basis for future investigations into real-time turbulence modeling. This goal was achieved; our extensive additions to the rotor model added less than a 10 percent computational overhead. Using a VAX 9000 computer the entire simulation required a cycle time of less than 12 msec.

Pilot opinion during this simulation was generally quite favorable. For low speed flight the consensus was that SORBET (acronym for title) was better than the conventional body-fixed model, which was used for comparison purposes, and was determined to be too violent (like a washboard). For high speed flight the pilots could not identify differences between these models. These opinions were something of a surprise because only the vertical turbulence component on the rotor system was implemented in SORBET. Because of the finite-element distribution of the inputs, induced outputs were observed in all translational and rotational axes. Extensive post-simulation spectral analyses of the SORBET model suggest that proper rotorcraft turbulence modeling requires that vertical atmospheric disturbances not be superimposed at the vehicle center of gravity but, rather, be input into the rotor system, where the rotor-to-body transfer function severely attenuates high frequency rotorcraft responses.

14. SUBJECT TERMS Rotorcraft, Turbulence, Blade element, Simulation			15. NUMBER OF PAGES 17
			16. PRICE CODE A03
17. SECURITY CLASSIFICATION OF REPORT Unclassified	18. SECURITY CLASSIFICATION OF THIS PAGE Unclassified	19. SECURITY CLASSIFICATION OF ABSTRACT	20. LIMITATION OF ABSTRACT

NSN 7540-01-280-5500

Standard Form 298 (Rev. 2-89)
Prescribed by ANSI Std. Z39-18
298-102